MORPHOLOGICAL TRANSFORMATIONS IN POLYMER BRUSHES IN BINARY MIXTURES: DPD STUDY

By

JIANLI CHENG

A thesis submitted to the

Graduate School-New Brunswick

Rutgers, The State University of New Jersey

in partial fulfillment of the requirements

for the degree of

Master of Science

Graduate Program in Chemical and Biochemical Engineering

written under the direction of

Dr. Alexander V. Neimark

and approved by

_____

_____

_____

_____

New Brunswick, New Jersey

Oct 2014

ABSTRACT OF THE THESIS

Morphological transformations in polymer brushes in binary mixtures: DPD study

By JIANLI CHENG

Thesis Director:

Professor Alexander V. Neimark

Morphological transformations in polymer brushes in a binary mixture of good and bad solvents are studied using dissipative particle dynamics (DPD) simulations drawing on a characteristic example of polyisoprene natural rubber (PINR) in acetone – benzene mixture. A coarse-grained DPD model of this system is built based on the literature experimental data available. We focus on the transformation of dense collapsed brush in bad solvent (acetone) to expanded brush solvated in good solvent (benzene) as the concentration of benzene increases. A coarse-grained DPD model of this system is built based on the literature experimental data available. Compared to a sharp globule-to-coil transition observed in individual tethered chains, collapsed-to-expanded transformation in brushes is found to be gradual without a prominent transition point. The transformation becomes more leveled as the brush density increases. At low densities, the collapsed brush is highly inhomogeneous and patterned forming bunches composed of neighboring chains due to favorable polymer-polymer interaction. At high densities, the

brush is expanded even in the bad solvent due to steric restrictions. In addition, we considered a model system similar to the PINR-acetone-benzene system, but with the interactions between the solvent components worsened to the limit of miscibility. Enhanced contrast between good and bad solvents facilitates absorption of the good solvent by the brush, shifting the collapsed-expanded brush transformation to lower concentrations of the good solvent. This effect is especially pronounced for higher brush densities.

Table of Contents

1. Introduction

Polymer brushes are composed of polymer chains that are attached to a solid surface by one end. Macromolecular brushes are ubiquitous in nature (for example, they provide lubrication of joints [1] and form periciliary layers that separate mucus layer from airway epithelia in lungs [2]) and find a broad range of practical applications, including stabilization of colloids and composites, mediating forces between solid, as cushions for supported lipid bilayers, [3] modification of chromatographic supports, [4, 5] ion-selective electrodes, [6] functionalization of surfaces for biomedical applications, [7, 8] and various particle and nanoparticle technologies. [9]

Polymer brushes respond to changes in chemical and physical environment (such as temperature, pH, solvent composition). In a thermodynamically good solvent the grafted chains are solvated and the brush swells. Depending on grafting density, the chains are stretched and form a layer of polymer solution at the substrate, which is called "expanded" state. In a thermodynamically poor solvent, the brush collapses into a dense melt-like layer on the substrate. Transition between the collapsed and expanded states is analogous to the globule-coil transition in a single tethered polymer chain. The difference is that polymer brushes are *dense*. That is, the distance between the attached chains is much smaller than the chain length, and therefore the structure of polymer brushes strongly depends on the grafting density. The other factors governing brush solvation are polymer interactions with solvent and solid substrate.

The conformations of polymer chains in a brush determine the interactions of polymer-grafted surfaces with other bodies, such as solid surfaces, colloidal particles, proteins, and macromolecules. Understanding of transitions between collapsed and

expanded configurations is therefore of critical importance for practical applications, and significant efforts were dedicated to this phenomenon. Collapsed-to-expanded transitions were extensively studied both experimentally [10, 11] and theoretically with molecular dynamics, [12] Brownian dynamics, [13] and dissipative particle dynamics (DPD) [14] simulations, as well as with density functional theory (DFT) [15] and self-consistent field theory (SCFT). [16, 17] It was found that collapsed brushes in bad solvents can be uniform (the polymer forms a homogeneous film adsorbed at the substrate) or patterned. Several regular and irregular pattern morphologies such as "octopus micelles", [13, 18] "pancake micelles", [19] or stripes [19, 20] were observed in various systems depending on their chemistry and composition. In a single-component solvent, a transition to an expanded configuration may be caused by a temperature increase, or chemically: for example, several theoretical studies of polyelectrolyte brushes [14, 16, 21-26] focus on the effect of charge density on the chains, which is controlled by the pH.

In multicomponent solvent, the solvent quality is commonly controlled by the solvent composition: the brush transits from a collapsed to an expanded configuration as the fraction of good solvent in the solvent mixture increases. Because brushes are dense, they may selectively absorb a particular component, even when both components are miscible. This effect can substantially affect polymer configurations compared to those in single-component solvents. Surprisingly, the theoretical literature on the brushes in binary solvents is rather sparse. [11, 15, 27-36] Brushes in binary solvents were studied theoretically by SCFT and DFT particular experimental systems were not targeted. The conditions of collapsed-to-expanded transitions were found to depend on the brush grafting density, polymer molecular weight, and specifics of polymer-solvent and

solvent-solvent interactions. In some systems, the conformational transitions were accompanied by sharp changes of solvent composition inside the brush. [32, 33, 35-37] Using de Gennes' mean-field theory, [38] Birshtein and Lyatskaya [29] considered with a brush in a bad solvent A, to which a good solvent B, miscible with A was gradually added. The transition between collapsed and swollen states was analogous to that in a single-component solvent with changes in temperature or solvent quality. Later, Birshtein et al [32] considered solvents had low mutual solubility. They found that the brush exhibited a first-order compositional transition characterized by spontaneous increase in height and adsorption of a good solvent. The authors also examined a conformational transition induced by an external deformation of the brush. [32, 34] Lyatskaya and Balasch [31] in their SCFT study considered water sorption from oil-water mixture by dense hydrophilic brushes including a weakly acidic polymer that was allowed to dissociate. The water concentration in the mixture was shown to control the effective brush height, and the local density of polymer segments has a maximum at the interface that formed between the hydrophilic layer that consisted of water and hydrophilic polymer and the hydrophobic oil bulk. Amoskov et al [39] also theoretically modeled polymer brushes in binary solvents limited miscibility. The equilibration between the brush and the solvent bulk was restricted using a membrane.

Borowko and Staszewski [15] used classical DFT model with Lennard-Jones (LJ) interactions between polymer and solvent particles. They focused on the selective adsorption of a better solvent by the brush, whose condition was characterized by effective brush height. Polymer length was fixed to 18 LJ monomers, while brush density, solvent composition and depth of LJ potential between solvents, polymer and

wall were varied. No spontaneous transitions between the collapsed and extended configurations were observed. Interestingly, the brush height showed a non-monotonic variation with solvent composition, which was explained by the balance of entropic repulsion forces between the polymer chains and solvent-polymer attraction for brushes of relatively low density.

In this paper, we investigate with dissipative particle dynamics (DPD) simulations the behavior of brushes of different grafting densities in a binary mixture of good and bad solvents. We explore the evolution of the brush structure and the solvent concentration within the brush, as the solvent composition changes. Calculations are performed for a realistic system, polyisoprene natural rubber (PINR) in acetone – benzene mixture, which provides an opportunity for correlation with experiments. Polyisoprene chains are commonly used for functionalization of particles of various sizes and chemistry, including macroscopic silica particles applied in rubber tires, [40] polymeric and metal particles for nanocomposites, [41, 42] and even single-wall carbon nanotubes. [43] Acetone (A) and benzene (B) are common solvents, which are mutually miscible at ambient conditions; acetone is a bad solvent [44] and the benzene is a good solvent [45] for PINR.

2. Simulation Methodology

2.1 Outline of DPD method

The DPD method is a simulation technique for hydrodynamic modes which can fill the gap between the nanoscale simulation and the macrosacle simulation. One prominent advantage in DPD method is that it can speed up the most time-consuming part of a simulation based on the coarse-grained strategy utilized to map a few groups into a single unit so that fewer particles will be looped over compared with the ordinary molecular dynamics (MD). Another major advantage is that we can assign much larger time-steps in DPD simulation as the pairwise interactions between particles are based on soft repulsion potential and are allowed to be overlapped. The increase of the time-steps results in a higher computational efficiency.

The system dynamics and equilibration is monitored by solving the equations of motion for the beads, and the time evolution obeys the Newton's equations of motion and the force acting on every particle is governed by three pairwirse short range components: a conservative force F^C, a drag force F^D, and a random force F^R:

$$\frac{d\boldsymbol{r_i}}{dt} = \boldsymbol{v_i}, \frac{d\boldsymbol{v_i}}{dt} = \boldsymbol{f_i} = \sum_{j\neq i}\left(\boldsymbol{F_{ij}^C} + \boldsymbol{F_{ij}^D} + \boldsymbol{F_{ij}^R}\right)$$

where the sum loops over all the neighboring beads within an assigned cutoff R_c, which is the effective bead diameter. The mass for every bead is put at 1, then the acceleration of each bead equals to its force f_i. The soft repulsive conservative force depends on the positions between beads i and j and is given by:

$$\boldsymbol{F_{ij}^C} = -a_{ij}\left(1 - \left|\boldsymbol{r_{ij}}\right|/R_C\right)\hat{\boldsymbol{r}}_{ij},\ \ at\ \left|\boldsymbol{r_{ij}}\right| < R_C;\ \boldsymbol{F_{ij}^C} = 0, at\ \left|\boldsymbol{r_{ij}}\right| \geq R_C$$

where a_{ij} is the repulsion parameter and depends on bead types i and j to which beads i and j belong; and $\hat{\boldsymbol{r}}_{ij}$ is a unit vector at the direction of $\boldsymbol{r_{ij}}$, where $\boldsymbol{r_{ij}} = \boldsymbol{r_i} - \boldsymbol{r_j}$, $\hat{\boldsymbol{r}}_{ij} = \boldsymbol{r_{ij}}/|\boldsymbol{r_{ij}}|$.

The drag force and the random force are combined to serve as a Langevin thermostat. They are given by:

$$\boldsymbol{F_{ij}^D} = -\gamma w^D(r_{ij})(\hat{\boldsymbol{r}}_{ij} \cdot \boldsymbol{v_{ij}})\hat{\boldsymbol{r}}_{ij}, \quad \boldsymbol{F_{ij}^R} = \sigma w^R(r_{ij})\theta_{ij}\hat{\boldsymbol{r}}_{ij}$$

where $\boldsymbol{v_{ij}} = \boldsymbol{v_i} - \boldsymbol{v_j}$, and $w^D(r_{ij})$ and $w^R(r_{ij})$ are weight functions of $\boldsymbol{F_{ij}^D}$ and $\boldsymbol{F_{ij}^R}$ forces respectively. They are related to satisfy fluctuation-dissipation theorem: $w^D(r) = [w^R(r)]^2 = (1-r)^2$ for $r < 1$ and $w = 0$ for $r > 1$. $\theta_{ij}(t)$ is a Gaussian fluctuating variable to give an random value to $\boldsymbol{F_{ij}^R}$ at each time-step. There is also a relation between the dissipation strength γ and noise strength σ as $\sigma^2 = 2\gamma k_B T$, and k_B is the Boltzmann constant. Follwing Groot and Warren [46], we assign $\sigma = 3$. The drag force works to decrease the relative velocity between beads i and j, on the contrary, the random force tends to increase this velocity. They are balanced to fix the temperature of the system. This thermostat is special in its conservation of momentum and therefore can preserve hydrodynamics. We choose the units of mass, energy and length as: $m = k_B T = R_C = 1$. Accordingly, the unit of time is given by: $\tau = R_C\sqrt{m/kT}$

In DPD method, a modified version of the velocity-Verlet algorithm [46] is introduced to update the positions and velocities $(\boldsymbol{r_i}, \boldsymbol{v_i})$ at every time-step and integrate the equation of motion:

$$\boldsymbol{r_i}(t + \Delta t) = \boldsymbol{r_i}(t) + \Delta t \boldsymbol{v_i}(t) + \frac{1}{2}(\Delta t)^2 \boldsymbol{f_i}(t),$$

$$\tilde{\boldsymbol{v}}_{\boldsymbol{i}}(t + \Delta t) = \boldsymbol{v_i}(t) + \lambda \Delta t \boldsymbol{f_i}(t),$$

$$\boldsymbol{f_i}(t+\Delta t) = \boldsymbol{f_i}\big(\boldsymbol{r}(t+\Delta t), \tilde{\boldsymbol{v}}(t+\Delta t)\big),$$

$$\boldsymbol{v_i}(t+\Delta t) = \boldsymbol{v_i}(t) + \frac{1}{2}\Delta t\big(\boldsymbol{f_i}(t) + \boldsymbol{f_i}(t+\Delta t)\big).$$

The force is updated once per integration and because it depends on the velocity, we use $\tilde{\boldsymbol{v}}_{\boldsymbol{i}}(t+\Delta t)$ as the prediction of the velocity of a particle at time $t+\Delta t$. The velocity is corrected in the last step. If the force does not depend on the velocity, $\lambda = 0.5$ and the algorithm is turned back to velocity-Verlet algorithm. [47]

2.2 Models and simulation parameters

As a characteristic example for our study, we selected polyisoprene natural rubber (PINR) and a mixture of acetone (A) and benzene (B). Acetone and benzene are mutually miscible; acetone is a bad solvent [44] and benzene is a good solvent [45] for PINR. In a setup standard for DPD simulations [46, 48], we represented the polymer as a sequence of soft beads connected by harmonic bonds $\mathbf{F}_{ij}^{(\mathrm{B})} = -K_I^{(\mathrm{B})}(r_{ij} - r_e)(\mathbf{r}_{ij} / r_{ij})$, where $K^{(\mathrm{B})}$ is the bond strength and r_e is the equilibrium distance. The system dynamics and equilibration is monitored by solving the equations of motion for the beads, which interact through pair-wise short range conservative, drag, and random forces.

We used the most common formulation of the DPD method, [46] which implies that the same effective diameter R_c for all system components and same intra-component repulsion parameter $a_{\mathrm{II}} = a_{\mathrm{AA}} = a_{\mathrm{BB}} = a_{\mathrm{PP}}$. The reduced density ρ^* of DPD beads (the average number of bead centers in $1R_C^3$) was set to $\rho^* = 3$, and the friction coefficient γ was set to 4.5 as recommended in ref [46] (note that dynamic properties are not

considered here). The system parameters were customized to mimic the properties of PINR, benzene and acetone.

2.2.1 Choosing R_c and a_{II}

In the most of DPD simulations, the system parameterization is based on the DPD parameters for water recommended in the original papers of Groot and Warren. [46] Here, we dealt with a purely organic system. Keeping in mind the DPD water parameters as a reference, we derived the coarsed-grained parameters from the properties of organic compounds involved.

We model PINR as a chain of beads P representing one monomer and solvents with beads A and B representing one molecule of acetone or benzene. The bead diameter R_c was determined from the effective volumes of PINR monomer, benzene and acetone molecules provided the reduced system density of 3. These volumes, calculated from the densities at ambient conditions and presented in Table S1 of Supporting Information, are relatively close and yielded the effective R_c values ranging from 0.71nm to 0.76nm. The bead size was chosen as R_c = 0.71nm. This value corresponds to the bead diameter of water coarse-grained as four water molecules per bead. [46]

The intra-component repulsion parameter was estimated from the ambient isothermal compressibility κ_T of the solvent by interpolation of experimental value onto the reference correlation between $1/\kappa_T$ and a_{II} [46] obtained in a separate series of DPD simulations (the reference curves R_c = 0.71nm is given in Supporting Information to ref [49]). This procedure produced values of $a_{II} = 36kT/R_c$ for acetone and $a_{II} = 48kT/R_c$ for benzene. Because the values are relatively close and compressibility has to be reproduced only approximately, we chose the mean value of $a_{II} = 42kT/R_c$.

2.22 Rigidity of the PINR chain

The rigidity of molecules may substantially influence the solution properties. [50] The chain rigidity determines the persistence length and therefore affects the polymer brush height and gyration radius. The bond strength $K^{(B)}$ and equilibrium distance r_e of the DPD model were fitted to semi-quantitatively reproduce the chain conformations in the atomistic molecular dynamic (MD) simulation. To this end, we performed NPT MD simulations of PINR melt. The details are described in Appendices, section A2. PINR is a rubbery polymer, liquid-like at ambient conditions. We simulated a melt of PINR oligomers, each of which contained sixteen monomers, using OPLS united-atom forcefield [51] and M.DynaMix software. [52] In DPD simulations, each oligomer was modeled as a linear chain of sixteen beads. From MD trajectory saved to the disk, we calculated the center of mass of each monomer and obtained the distribution of distances between the neighboring monomers (1-2 distance), second and third neighbor monomers separated by one (1-3 distance) and two (1-4 distance) monomers. The obtained distributions are shown in Figure 1. It is clear that the maximum probability for the effective 1-3 (second-neighbor) and 1-4 distances do not commensurate with nearest neighbor (1-2) distance: $r_{1\text{-}3} < 2r_{1\text{-}2}$, $r_{1\text{-}4} < 3r_{1\text{-}2}$. Furthermore, both distances show two maxima, indicating a complex conformational behavior. This means that straight conformation is not preferential even at the small scale, and therefore the persistence length is very short, less than 8 covalent bonds that separate the centers of second-neighbor beads. This behavior of PINR is dissimilar to alkanes and other simple chain molecules, such as perfluoroalkanes (for which these distributions are given for comparison in Supporting Information, Figure S1). Because of the short persistence

length and inability of the standard models with second-neighbor bonds and covalent angles [50] to reproduce the complex shape of PINR, we decided to use only the nearest neighbor 1-2 bonds with the parameters $K^{(B)}$ and r_e fitted to the MD results, see Table 1 and Figure 1.

Short-range conservative repulsion parameters a_{IJ}, kT/R_c				
Bead type	S	P	A	B
S	42.0	42.0	42.0	42.0
P	42.0	42.0	49.0	43.5
A	42.0	49.0	42.0	43.5 (s. I) 49.0 (s. II)
B	42.0	43.5	43.5 (s. I) 49.0 (s. II)	42.0
Chain length and bond parameters				
$N = 100$	$K^{(B)} = 120\ k_BT/R_c^2$		$r_e = 0.57$ nm	

Table 1. Parameters of the coarse-grained models for systems I and II. Denotation of beads: S - substrate, P - PINR monomer, A – bad solvent, and B - good solvent.

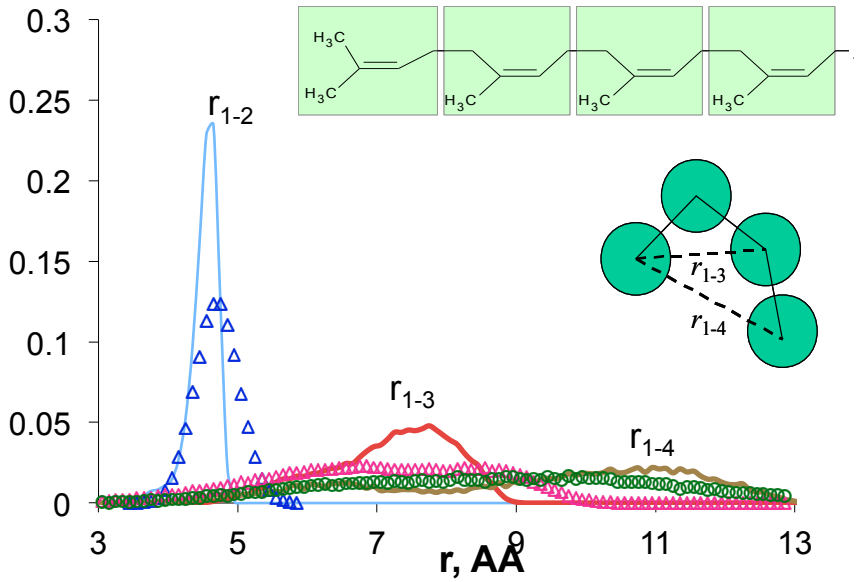

Figure 1. The model of polyisoprene natural rubber (PINR) and distributions of the distances between the near neighbor $r_{1\text{-}2}$, second neighbor $r_{1\text{-}3}$, and third neighbor $r_{1\text{-}4}$ monomers in PINR oligomer obtained in MD simulation (lines) and DPD (points).

2.2.3 Inter-component repulsion parameters

The a_{AB}, the parameter of short-range repulsion between acetone and benzene, was calculated from experimental value of infinite dilution activity coefficient (IDAC) of benzene solved in acetone γ_∞ = 1.70 found in [53] using the method suggested by us earlier in ref [54]. The method is based on the fit to the experimental value of the theoretical IDAC determined by the Monte Carlo Widom insertion technique for given binary system of A and B beads. The correlation between a_{AB} and IDAC is described in Appendices, Section A-4, Figure A3. Thus, we obtained the mismatch paramter Δa_{AB} = a_{AB} - a_{II} = 1.5 kT/R_c, and respectively, a_{AB} = 43.5kT/R_c.

For polymer solvent interactions, IDAC values were not found in the literature, but the dependences of solvent activity on concentration $a(c)$ were given in ref [45] for

benzene and ref [44] for acetone. Benzene and PINR are miscible, and $a(c)$ is accurately described by the Flory-Huggins (FH) equation of state with a single FH parameter χ_{BP} = 0.42 independent on c. (Figure 2). We used a standard correlation $\Delta a_{BP} = \chi_{BP}/0.286$ [46] to obtain benzene-polymer parameter $a_{BP} = 43.5kT/R_c$.

For poor solvent acetone, the FH parameterization was not possible, because the χ_{AP} estimated by Booth et al. [44] drastically increased with the fraction of polymer in the mixture, and our attempts to fit the experimental data with the FH equation did not produce a satisfactory fit and underestimated the solubility of acetone in PINR (Figure 2). For this reason, we performed the parameterization using the MC simulation with Widom insertions [55] of an acetone bead into the DPD model of the solutions of 60-mer PINR oligomers and acetone. We performed several series of simulations with different polymer-solvent compositions and varying a_{AP}. We found that with $a_{AP} = 49\ kT/R_c$, the coarse-grained model described the experimental activities pretty well, and the solubility limit is also in a good agreement with experimental data. The details of respective MC simulations are described in Appendices, section A-3

The model with the parameters fitted to experimental parameters of the PINR-acetone-benzene-system, will be referred to as system I. We have to note that the solvents are very well miscible. In order to explore how an increase of the contrast of solvent quality affects the polymer brush solvation, we also considered a model system where the solvents are more dissimilar yet still miscible. According to ref [56], as well as our own DPD simulations, the maximum Δa at which a symmetric mixture shows no phase separation is close to 7.5 kT/R_c. We therefore chose $a_{AB} = 49kT/R_c$ to model the mixture

of two dissimilar yet miscible solvents, with all other parameters remaining the same. This system is referred to as system II. All parameters are summarized in Table 1.

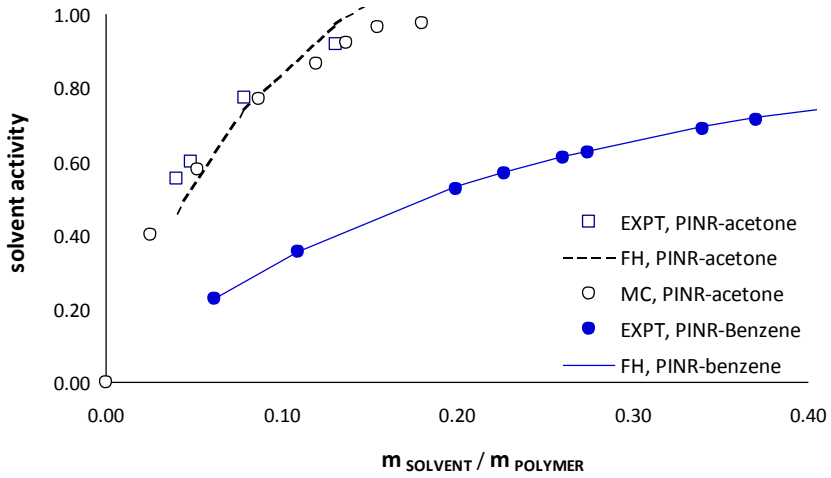

Figure 2. Dependence of solvent activity on composition for PINR-acetone (open symbols, dashed line) and PINR-benzene (closed symbols, solid line) mixture at T = 298K and P = 1atm. Experimental results [44, 45], fit with the Flory – Huggins model and Monte Carlo simulations with a_{PA} = 49kT/R_c, which produces the best fit to experimental data for PINR-acetone mixture.

2.2.4 Simulation setup

The solid substrate was formed by seven parallel layers of immobile beads at an effective density of 19.3 R_c^{-3}. a_S = 42 kT/R_c parameters were assigned to substrate interactions with all other bead type. Because of the high density of the substrate, it effectively repelled all other beads and had no preference to a polymer or either solvent. The polymer chains that form the brush consisted of 100 beads and were attached to the substrate in a square lattice order. The substrate area was about 30x30 R_c^2 (21.3x21.3nm), and the distance between the neighboring chains was varied from 4 to 1.5 R_c, which

corresponds to brush densities of 0.12, 0.16, 0.32, 0.50 and 0.88 nm^{-3}. That is, in the least dense brushes, the distance between the chains was compared to the radius of gyration of an individual tethered chain placed in a good solvent, while in the densest brushes this distance was comparable to the bead diameter. Other details of DPD simulations may be found in Appendices, section A-5.

3. Results and Discussion

3.1 Collapsed to expanded transformation in polymer brushes

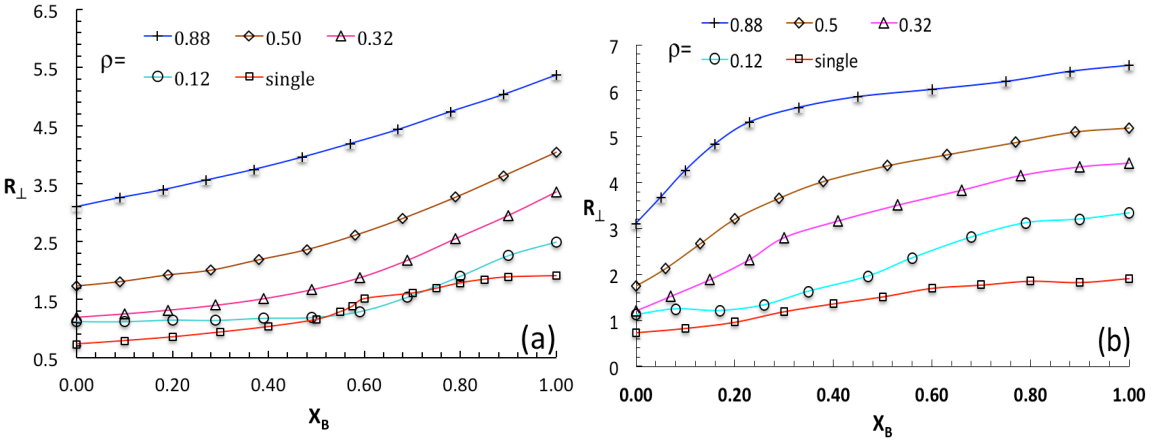

Figure 3. Normal to the surface radius of gyration of polymer chains in brushes of different grafting densities as a function of the good solvent mole fraction x_B in the equilibrium bulk mixture. (a) System I – PINR-acetone-benzene. Note gradual collapsed-to-expanded transformations in polymer brushes compared to the stepwise globule-coil transition for single chains. The brush height sharply increases with the grafting density due to the inter-chain interactions. (b) System II – same system with an enhanced contrast between good and bad solvent, see explanation in the text. The standard deviation of the normal radius of gyration for single chain ranges from 0.1 in pure acetone to 0.8 in pure benzene. The value of standard deviation is trivial for polymer chains in brushes.

Figure 3 shows the dependence of the normal radius of gyration for PINR polymers in acetone-benzene mixture (system I) at different brush densities and solvent compositions. A single PINR 100-mer-chain tethered to the substrate serves as a reference. The single chain exhibits a characteristic transition from a globule at the

substrate surface to a coil, signified by the increase of average normal radii of gyration $R_{\perp}$ from 0.73Rc in pure acetone (benzene mole fraction in the solvent bulk $x_B = 0$) to 1.91Rc in pure benzene ($x_B = 1$). The transition in the binary solvent is analogous to that in a one-component solvent with increase in temperature, for example. Normal and tangential radii of gyration $R_{\perp}$ and $R_{//}$ grow monotonically with x_B. The inflection point corresponds approximately to $x_B = 0.55$. The snapshots of the collapsed and expanded configurations of single tethered chains are given Figure 4 a) and b) and in Appendices, section A-6.

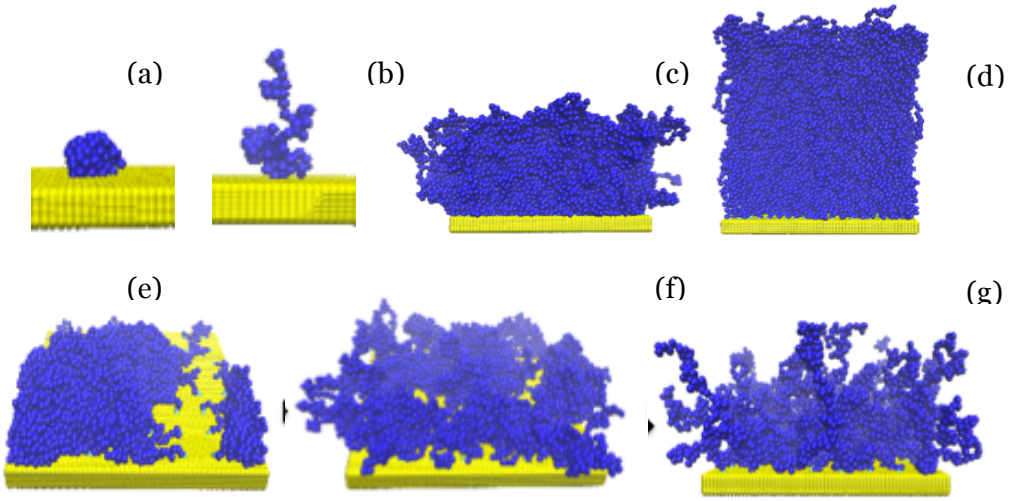

Figure 4. Snapshots of PINR brush conformation in binary solvent (solvent not shown). Top: low brush density of 0.12nm^{-2}. System I (a) globular single chain, $x_B = 0$, (b) coiled single chain, $x_B = 1$, (c) dense brush (0.88nm^{-2} system I) forms a uniform polymer layer in bad solvent, (d) dense expanded brush (0.88nm^{-2}, system I), (e) collapsed brush in a bad solvent, $x_B = 0$. The polymer layer is inhomogeneous with some areas of substrate exposed to the solvent, (f) semi-expanded brush at $x_B = 0.4$, (g) fully expanded brush in good solvent, $x_B = 1$.

Very different picture is observed for low-density polymer brushes. At, $x_B = 0$, the average normal radii of gyration $R_\perp$ of polymer chains at grafting densities of 0.12, 0.16 and 0.32 nm^{-2} are about $1R_c$, which suggests that the brushes are collapsed at the surface. At the same time, the overall radii of gyration (presented in Appendices, Figure A3) are comparable to the radius of gyration of a coil-like single chain at $x_B = 1$. Instead of forming individual globules, the chains are spread over the surface, forming a bigger aggregates (snapshots of which are given in Figure 4), apparently similar to the patterned configurations mentioned in the introduction. The size of our simulation cell is not sufficient to identify the pattern. We can only say that at low brush densities the polymer does not cover the entire surface; for example, a "parting" is seen in Figure 4e. As the quality of solvent improves with the increase of the benzene fraction x_B, R_g does not increase, despite a slowly growing $R_\perp$. This is because PINR chains become less stretched along the surface and the $R_{//}$ decreases with x_B. The brush forms globules, each of which is composed of several chains and swollen with benzene (Figure 4b), before finally transforming into a fully expanded configuration (Figure 4c). The presence of multiple chains apparently delays the collapsed-to-expanded transformation, which is less pronounced and happens at higher x_B compared to the coil-globule transition of an individual tethered chain.

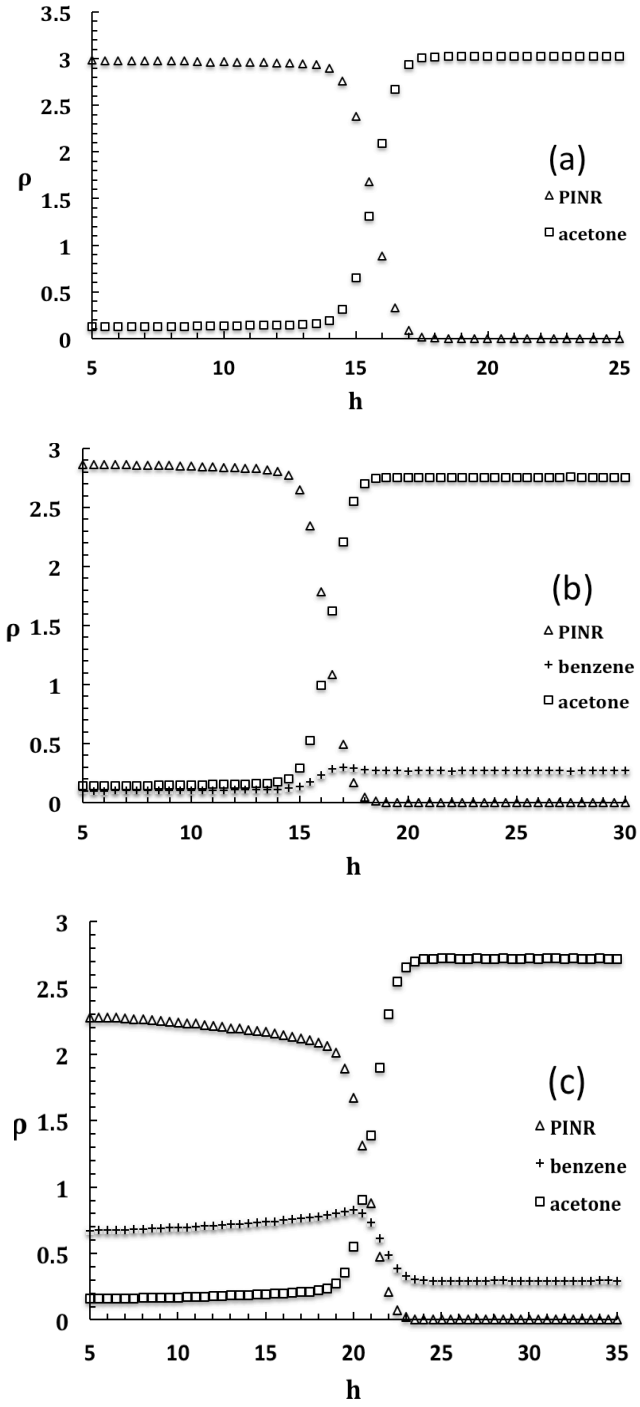

Figure 5. (a) Density profile for polymer brush and acetone in pure acetone at system I. Density profile for polymer brush, benzene and acetone at $x_B = 0.1$ in system I (b) and in system II (c).

As the brush density increases, the collapsed-to-expanded transformation becomes even less pronounced. For the denser brushes, the transition point could not be identified. Nevertheless, it appears that transformation form a collapsed to an expanded state is shifted towards lower x_B. In pure acetone, PINR forms a uniform layer at the surface, which preferentially absorbs benzene from the bulk, as demonstrated by the density and the solvent composition profiles, Figure 5a. Inside dense brushes, the average density of PINR monomers $\rho_P(z)$ remains relatively constant until it "drops-off" at the interface between the brush and the solvent bulk. Composition profile $y_B(z)$ (the average number of benzene beads in a unit volume located at distance z from the substrate related to the average number of all *solvent* beads) shows that benzene prevails inside the brush; the selectivity coefficient to benzene can be estimated as 10.2 at $x_B = 0.1$. However, the solvent composition profile inside the brush is never constant. In all systems, benzene fraction of solvent monotonically increases from the substrate towards the bulk, despite a maximum in absolute benzene concentration observed at the interface between the brush layer and bulk solvent in system II (see next section). Polymer beads showed no particular affinity to the interface between the brush and solvent bulk observed for immiscible solvents in earlier theoretical modeling. [31]

3.2 Influence of the interactions between the good and bad solvents.

Unlike actual acetone and benzene, the solvents in system II are barely miscible. As a result, the structure of the solvent bulk is locally inhomogeneous with "domain" of clustered A and B beads, although the mixture exhibits no macroscopic phase separation. While the interaction between solvents has almost now effect on the behavior of the individual chains, it strongly affects the collapsed-to-expanded transition in the brushes,

especially in dense ones: as the solvent-solvent interactions become less favorable, distribution coefficient of good solvent B between the brush and the bulk solvent mixture increases and the absorption becomes much more pronounced. Even in low-density brushes, the transition from patterned collapsed structures to swollen globules is observed at lower x_B. At $x_B = 0.5$, the chains of the least dense brush ($\rho_s = 0.12$ nm^{-2}) in system II have the same R_g as they have at $x_B = 0.85$ in system I. In the densest brushes ($\rho_s = 0.85$ nm^{-2}) the change in solvent-solvent interaction increases the selectivity coefficient of the surface from from 10.2 to 38.3 at $x_B = 0.1$. As a result, the brush shows a pronounced swelling and chain stretching (revealed by the increase in R_g) even at very low x_B, which was not the case in system I. The collapsed-to-stretched transition in the brush occurs between $x_B = 0$ and $x_B = 0.2$. After that, polymer chains extend slowly as the overall solvent quality improves further. Qualitatively, the density and the solvent composition profile remain similar to those in system 1: the density of polymer segments is constant inside the brush and shows a well-defined interface with the solvent bulk, while the good solvent shows a concentration maximum at the brush surface.

4. Conclusion

The results obtained with DPD modeling of PINR brush in benzene-acetone mixtures demonstrate the specifics of conformations of polymer brushes in binary solvents. The experimentally informed parameterization of the model provides an opportunity to test the conclusions obtained from the modeling against respective measurements once the latter become available.

We found that, compared to the globule-coil transition in single chains, the collapsed-to-expanded transformation in brushes occurs gradually and at higher fractions x_B of good solvent, especially at low grafting densities. This is in contrast with the earlier mean field modeling studies that predicted that the conformational transformations in brushes are rather similar to globule-coil transitions. The ability of chains to merge, forming bunches, "octopus" micelles, stripes, or other patterns, effectively stabilizes the collapsed state. The entropy gain per chain in however limited, since neighboring chains restrict available conformations of each other, effectively destabilizing the stretched state and therefore shifting the expansion towards higher x_B. Same effect could be seen in theoretical studies of Birshtein and Lyatskaya [29]. Worsening of interactions between the solvent components shifts the collapsed-to-expanded transformation in the opposite direction towards lower x_B, due to absorption of the good solvent within polymer chains.

In collapsed-to-expanded transformations in polymer brushes, just as globule-coil transitions in single chains, the gain in entropy overcomes cohesive forces between the polymer segments. The difference between a single chain and a brush may be looked upon as the difference between a chain and an array of chains, each of which can expand from a collapsed to an extended state. However, the inter-chain interference facilitated by

adsorption of good solvent makes the chain expansion a collective process that occurs gradually without prominent stepwise transitions. The rounded collapsed-to-expanded transformations may be explained by a lower free energy barrier (per chain in the brush) associated with chain expansion compared to globule-coil transition.

The behavior of polymer brushes in binary solvents is of a special significance for chromatographic separations on polymer grafted stationary phases. In particular, in the gradient elution chromatography [57, 58] , the separation is controlled by varying the solvent composition, which affects adsorption of solute components. The effect of solvent composition is expected to be more pronounced for separation of polymers, proteins, or nanoparticles, elution of which is restrained by their adhesion to grafted substrates. In this process, the collapsed-to-expanded transformation of grafted chains upon variation of solvent composition may significantly influence the solute partition between mobile and immobile phases.

The problem of interactions between polymer-grafted nanoparticles on various stages of nanocomposite processing represents a challenging and practically important extension of this work. While the length of grafted chains is smaller than the particle size and the particle concentration is sufficiently low, the conclusions of this work remain intact. However, the nanoparticle size and their concentration bring about additional scales that may change the qualitative behavior leading to nanoparticle aggregation induced by the conformational changes of grafted chains. Another interesting set of problems that involve conformational transformations in polymer brushes includes the interactions of grafted nanoparticles with substrates, lipid bilayers, and cells.

5. Appendices

A-1. Properties of pure compounds and resulting R_c parameters.

Table S1.

compound	M.W. [g/mol]	density [g/cm^3]	V, [Å^3] /molecule	Rc [Å]	k_T [1/Pa]
acetone	58.08	0.79	121.97	7.1	1.23 E-09[a)]
benzene	78.11	0.88	148.03	7.6	9.38 E-10[a)]
PI-NR	68.12	0.92	123.00	7.1	

[a)] ref [59]

A-2. Molecular dynamics simulations of skeleton rigidity.

To estimate the rigidity of PINR, we performed MD simulation of PINR melt at ambient conditions. We constructed olygomers each containing 8 isoprene monomers as shown in Figure 1 (man text). The simulation procedures were similar to those employed in refs. [2, 3, 5] We employed OPLS united atom forcefield [5] for liquid alkanes and alkenes, where each CHx group was presented by one Lennard-Joned pseudo-atom. The rigid bonds were constrained using SHAKE algorithm; in lieu of rigid covalent angles, rigid second neighbor bonds were introduced and also constrained by SHAKE as implemented in MDynaMix [52] software package. The box was cubic and contained 200 PINR oligomers. In the initial configuration, molecules were arranged in a lattice order at a low density of 0.005 g/cm^3. The system was then gradually contracted in a series of constant-temperature MD simulations at T = 303K maintained by a simple velocity scaling. After the density of 0.85g/cm^3 was achieved, the simulation proceeded at a constant pressure P = 1atm. T and P were maintained by the Nose-Hoover thermostat.

[60, 61] System equilibration was performed for 500 ps followed by additional 1 ns MD simulation, over which the system configuration was periodically saved to disc for analysis. This saved trajectory was converted to a trajectory of beads motion, with the coordinates of each bead assumed to coincide with those of the center of mass of the corresponding fragment.

Figure A1 shows the probability distribution for bead -- bead distances (1-2 distributions are for neighboring beads, 1-3 distributions are for second neighbor beads separated by 1 bead, and 1-4 are distributions for beads separated by 2 beads). The locations of maxima for 1-3 and 1-4 distributions do not commensurate with those for 1-2 distributions, showing that the chain has essentially no rigidity and therefore cannot be fitted with standard DPD models that include either harmonic angles with the equilibrium angle of 180 deg or 1-3 bonds. The corresponding distance distribution for perfluorohexadecane from REF is shown for comparison (Figure A1b)

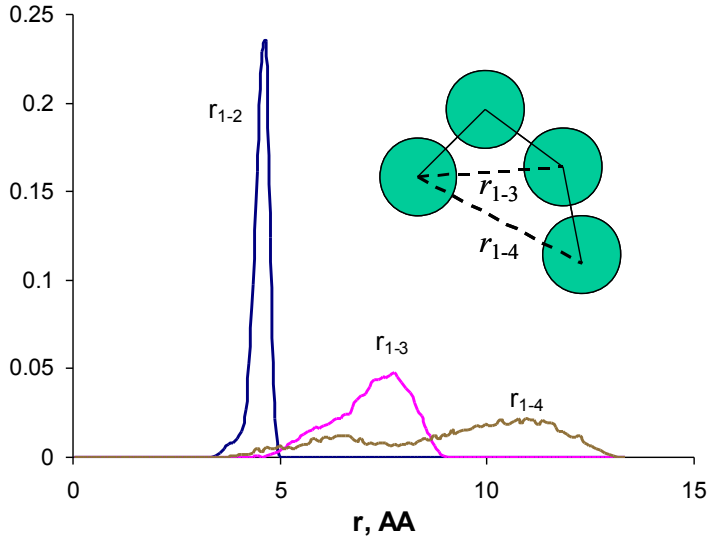

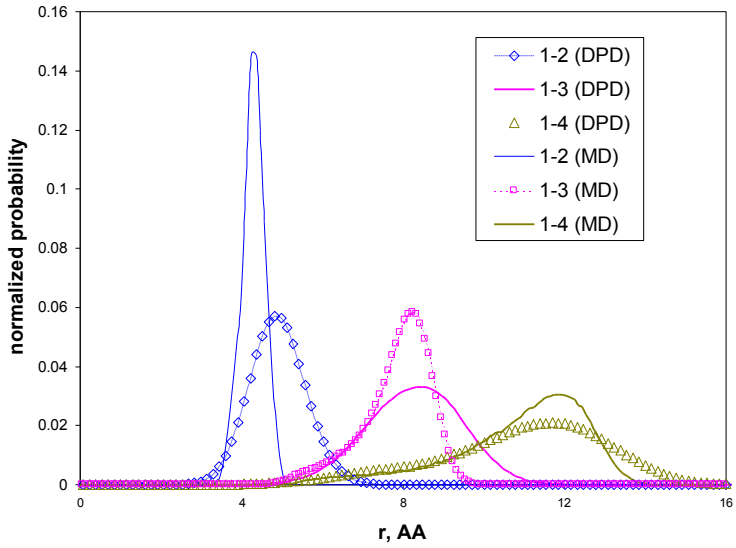

Figure A1. (a, top) distributions of distances between the intrachain beads in a PINR oligomer ar 298K (b, bottom) same for perfluorohexadecane at 450K and DPD fit.

A-3. Experimental data on solvent interactions with PINR and modeling with UNIFAC Free Volume and Flory-Huggins equations

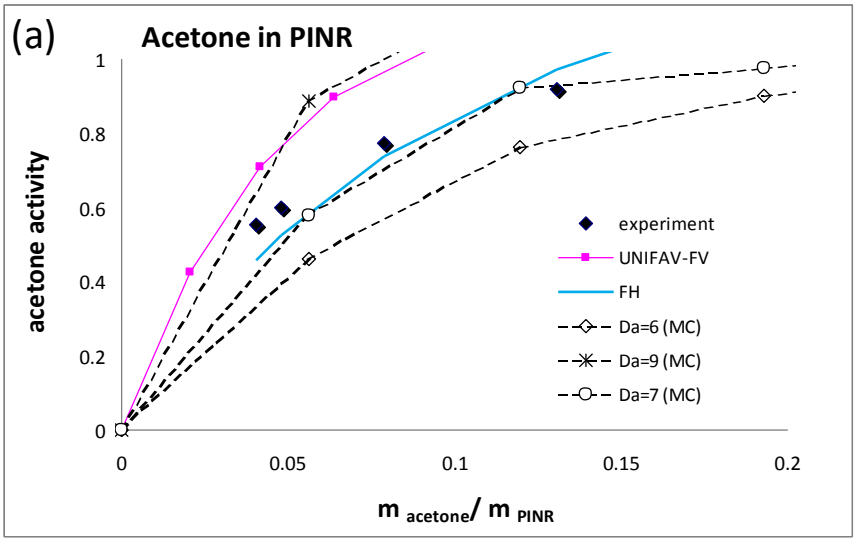

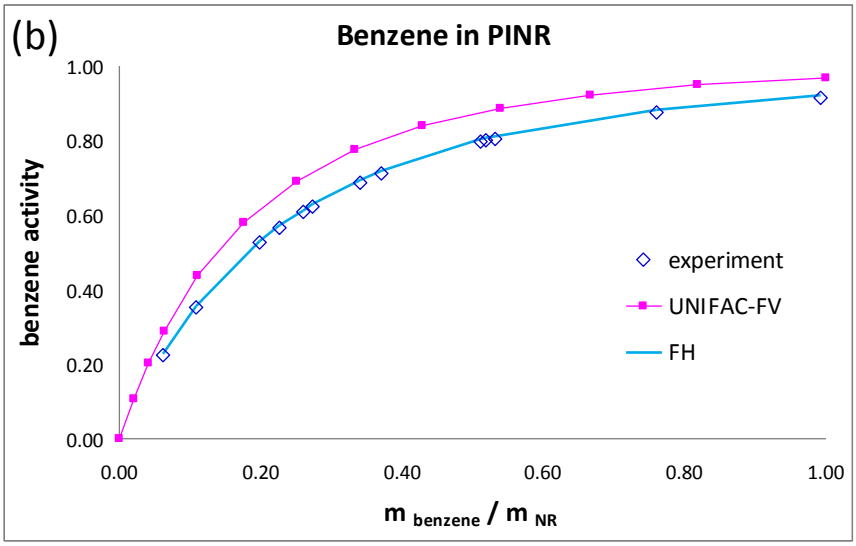

Figure A2. Experimental activities of acetone (a) and benzene (b) in PINR as a function of solvent mass related to polymer mass. Experimental data are replotted from refs [44, 45]; Flory-Huggins results are obtained by treating polymer chains as infinite at χ for polymer-solvent interaction as an adjustable parameter. The best fit is obtained with $\chi = 0.43$ in PINR -- benzene and $\chi = 1.5$ in PINR – acetone system, with still does not produce a good fit. MC simulations are described below. UNIFAC-FV results obtained with parameters from REFS and no fitting specific to the solutions considered in this work

A-4. Obtaining acetone-PINR conservative repulsion parameters using Monte Carlo simulations

The short-range repulsion parameter *a* for PINR-acetone system was obtained using Monte Carlo simulations in canonical (NVT) ensemble with random Widom insertion. PINR was presented by 60-mers, the box was cubic and 3D-periodic with $20R_c$ side and the only move type was random displacement; maximum displacement was

chosen to obtain 50% acceptance probability. The initial condition was random with 10^7 equilibration steps and $5*10^7$ averaging steps. During the averaging trial Widom insertions of acetone beads were performed, 10 insertions per displacement. Chemical potential of solvent was calculated with the standard Widom expression and converted to activity as $m = m_0 + RT \ln a$, where m_0 is the chemical potential of pure coarse-grained acetone, which was obtained in a separate simulation with acetone bead insertion in a bath of acetone beads. The best fit to the experiment was obtained by changing a parameter for PINR – acetone interaction manually, without a special iteration procedure. The results are shown in Figure S3.

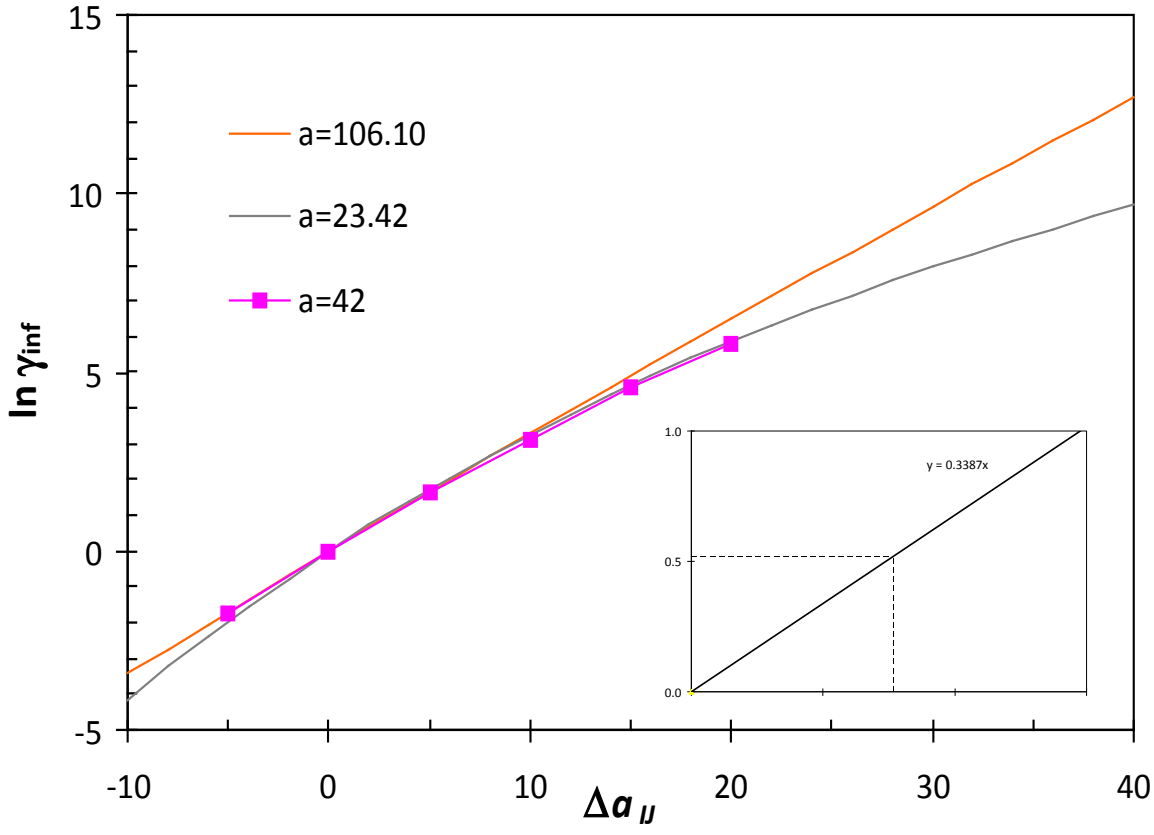

Figure A3. Dependence of the infinite dilution activity coefficient on the mismatch between intra- and inter- component interaction parameters obtained by Widom insertion

MC for intracomponent parameters a_{II} = 42kT/R_c. Results for a_{II} = 106.5 kT/R_c and a_{II} = 23.5 kT/R_c [54] are given for comparison. The interaction parameter is obtained by interpolation of experimental activity coefficient onto the refrence curve as shown by the insert on the right.

A-5. Details of DPD simulations

PINR was presented by oligomers each containing 100 monomers. Bead density $r*R_c^3$ in the fluid was set to 3, a common choice for non-aqueous solutions. The random force, which accounts for thermal fluctuations, is taken proportional to the conservative force that is also acting along the vector between the bead centers: $\boldsymbol{F}_{ij}^{(R)}(r_{ij}) = s w^R r_{ij} q_{ij}(t) \mathbf{r}_{ij}$, where $q_{ij}(t)$ is a randomly fluctuating in time variable with Gaussian statistics. The drag force is velocity-dependent: $\boldsymbol{F}_{ij}^{(D)}(\mathbf{r}_{ij}, \mathbf{v}_{ij}) = -g w^D(r_{ij}) (\mathbf{r}_{ij} * \mathbf{v}_{ij})$, where, $\mathbf{v}_{ij} = \mathbf{v}_j - \mathbf{v}_i$, $\mathbf{v}_i$ and $\mathbf{v}_j$ are the current velocities of the particles. We assume the common relationship between the drag and random force parameters $w^D(r) = [w^R(r)]^2$. s and g are parameters that determine the level of energy fluctuation and dissipation; they are related as and $s^2 = 2gkT$ that allows to maintain constant temperature in the course of simulation.

The solid substrate was formed by five parallel layers of immobile beads at an effective density of 5 R_c^{-3}. a_S = 42 kT/R_c parameters were assigned to substrate interactions with all other bead type. Because of the high density of the substrate, it effectively repelled all other beads and had no preference to a polymer or either solvent. The simulation box was cubic, 30x30x60R_c^3 in size. In the initial configuration, polymer chains were aligned in direction normal to the substrate, the distance between the neighboring beads was 0.25R_c. The solvent beads were places randomly. The simulation consisted of 1,000,000 DPD steps. After 500,000 steps, all coordinates were saved to disk

once in 500 steps. Density profiles and polymer gyration radii were calculated from the saved trajectories. DPD timestep was 0.02 in reduced time units. LAMMPS software [62] was employed to perform DPD simulations.

A-6. Collapsed-to-stretched transitions in polymer brushed. Snapshots from DPD simulations and radii of gyration

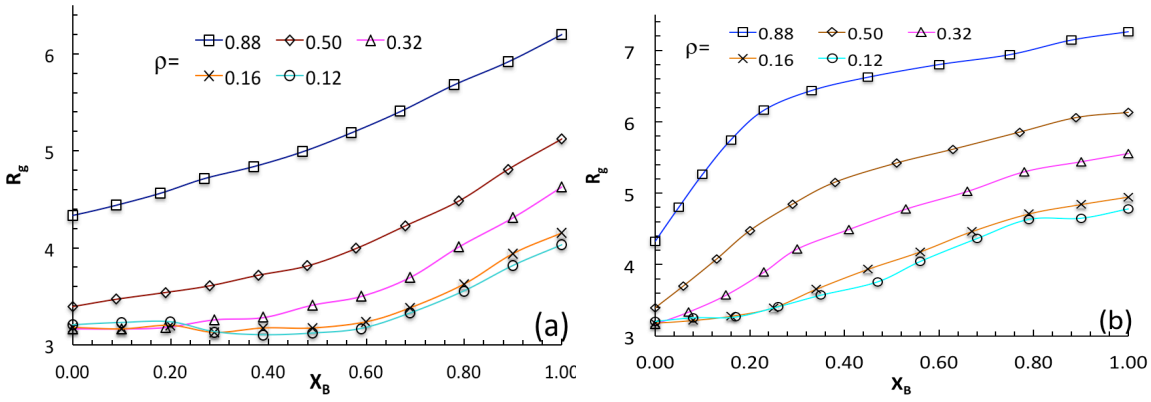

Figure A4. Overall radius of gyration of polymer chains in brushes of different grafting densities as a function of the good solvent mole fraction x_B in the equilibrium solvent bulk: system I (a) and system II (b).

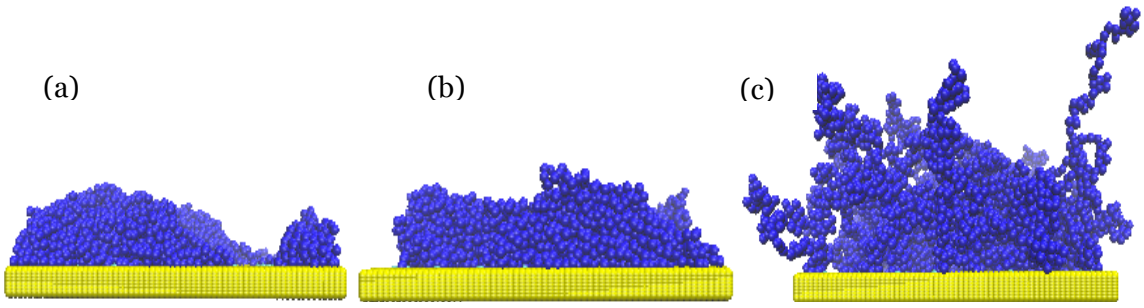

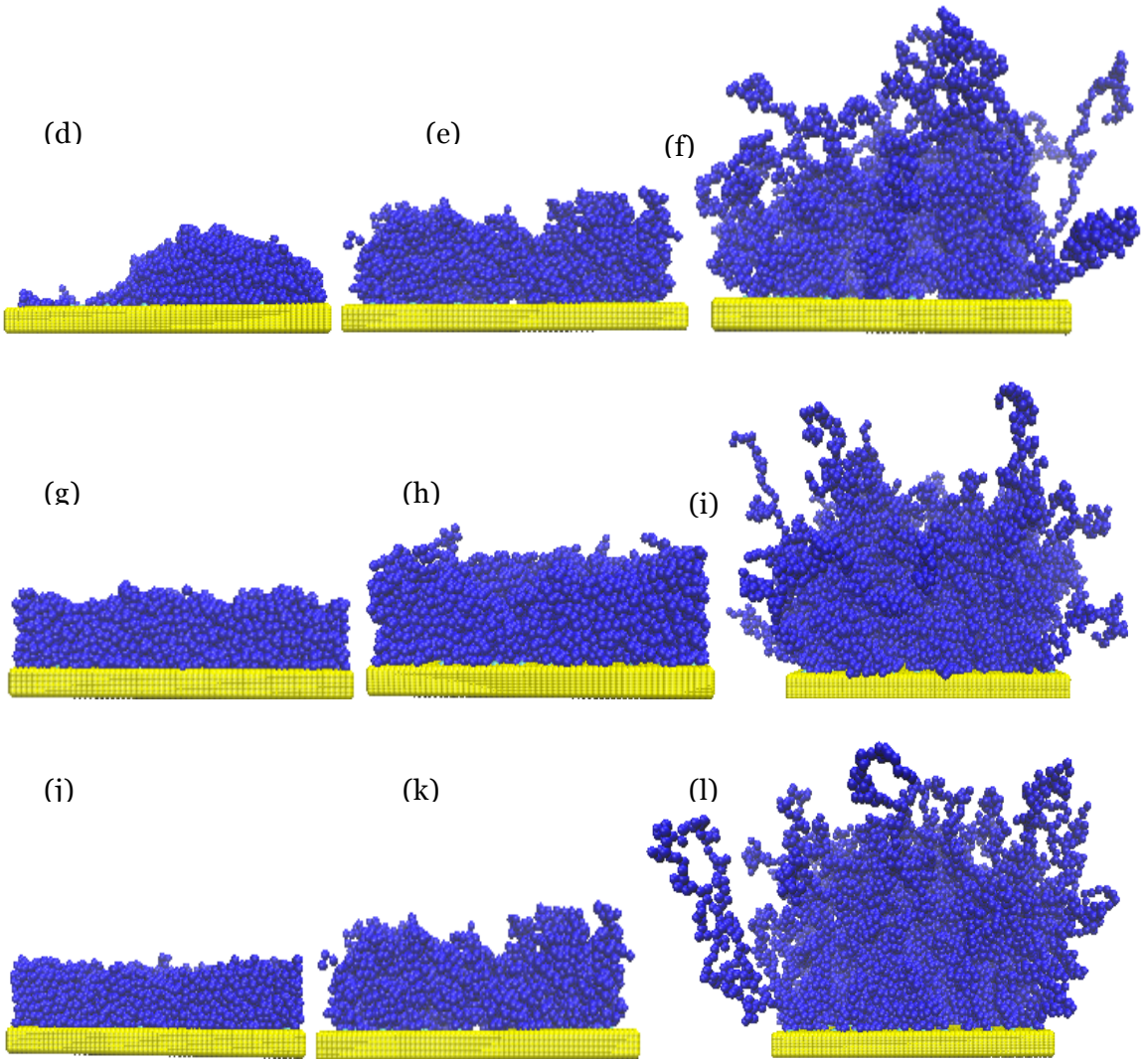
(d)
(e)
(f)
(g)
(h)
(i)
(j)
(k)
(l)

(m) (n)

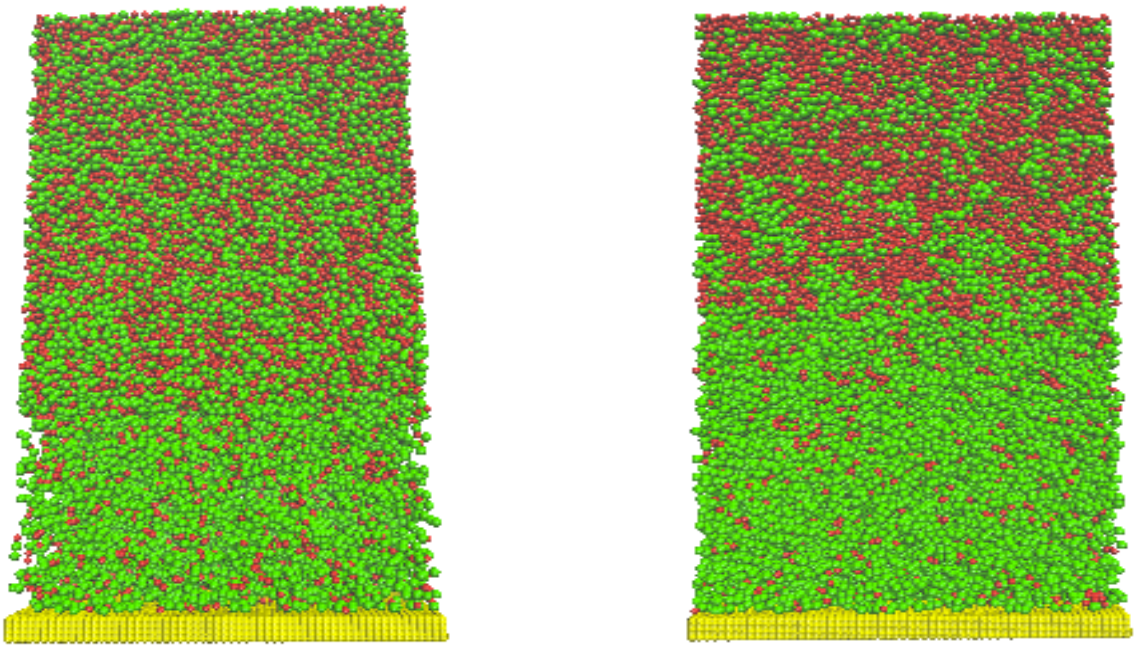

Figure A5. Snapshots of PINR brush conformation in binary solution (solven not shown). System I: low brush density of 0.12nm^{-2}: (a) collapsed brush in a bad solvent, $x_B = 0$. The polymer layer is inhomogeneous with some areas of substrate exposed to the solvent; (b) semi-stretched brush at $x_B = 0.4$; (c) fully stretched brush in good solvent, $x_B = 1$. Brush density of 0.3nm^{-2}: (g) collapsed brush phase at $x_B = 0$. The polymer layer fully covers the substrate surface; (h) collapsed brush starts swelling at $x_B = 0.4$; (i) fully stretched brush at $x_B = 1$. System II: low brush density of 0.12nm^{-2}: (d) collapsed brush phase at $x_B = 0$, the same as (a); (e) semi-stretched brush at $x_B = 0.4$. The brush has higher radii of gyration compared to (b); (f) fully stretched brush at $x_B = 1$. Brush density of 0.3nm^{-2}: (g) collapsed brush phase at $x_B = 0$. The brush forms a homogeneous layer to cover the substrate surface; (h) collapsed brush is swelling at $x_B = 0.4$; (i) fully stretched brush at $x_B = 1$. Snapshots of acetone (red) and benzene (green) distribution for system I (m) and

system II (n) at x_B = 0.5. The benzene molecules tend to stay close to substrate surface and more benzene molecules are attracted by polymer brush in system II.

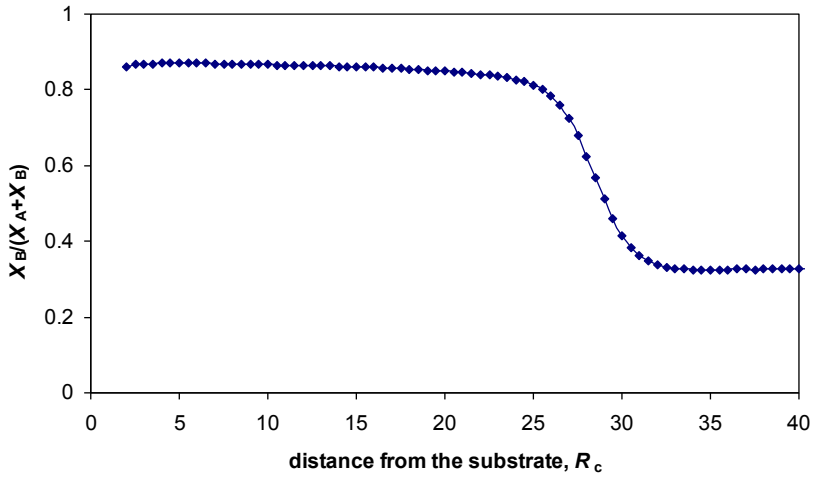

Figure A6. Solvent composition profile (benzene mole fraction) in system II, x_B = 0.33

6. References

1. Klein, J., *Molecular mechanisms of synovial joint lubrication*. Proceedings of the Institution of Mechanical Engineers Part J-Journal of Engineering Tribology, 2006. **220**(J8): p. 691-710.
2. Button, B., et al., *A Periciliary Brush Promotes the Lung Health by Separating the Mucus Layer from Airway Epithelia*. Science, 2012. **337**(6097): p. 937-941.
3. Parikh, A.N. and J.T. Groves, *Materials science of supported lipid membranes*. Mrs Bulletin, 2006. **31**(7): p. 507-512.
4. Mizutani, A., et al., *Thermo-responsive polymer brush-grafted porous polystyrene beads for all-aqueous chromatography*. Journal of chromatography A, 2009. **1217**(4): p. 522-529.
5. McCauley, B., et al., *Liquid Chromatography of Nanomaterials: Separation of Nanoparticles According To Surface Area and Chemistry* in *HPLC 2012. 38th International Symposium on High Performance Liquid Phase Separations and Related Techniques*2012: Anaheim Marriott Anaheim, CA USA. p. P-213.
6. Sempionatto, J.R., L.C. Recco, and V.A. Pedrosa, *Polymer Brush Modified Electrode with Switchable Selectivity Triggered by pH Changes Enhanced by Gold Nanoparticles*. Journal of the Brazilian Chemical Society, 2014. **25**(3): p. 453-459.
7. Halperin, A., M. Tirrell, and T.P. Lodge, *Tethered chains in polymer microstructure*. Advances in Polymer Science, 1992. **100**: p. 31-71.
8. Kawai, T., K. Saito, and W. Lee, *Protein binding to polymer brush, based on ion-exchange, hydrophobic, and affinity interactions*. Journal of Chromatography B-Analytical Technologies in the Biomedical and Life Sciences, 2003. **790**(1-2): p. 131-142.
9. Prokhorova, S.A., et al., *Can polymer brushes induce motion of nano-objects?* Nanotechnology, 2003. **14**(10): p. 1098-1108.
10. O'Shea, S.J., M.E. Welland, and T. Rayment, *An atomic-force microscope study of grafted polymers on mica*. Langmuir, 1993. **9**(7): p. 1826-1835.
11. Mir, Y., P. Auroy, and L. Auvray, *Density profile of polyelectrolyte brushes*. Physical Review Letters, 1995. **75**(15): p. 2863-2866.
12. Grest, G.S. and M. Murat, *STRUCTURE OF GRAFTED POLYMERIC BRUSHES IN SOLVENTS OF VARYING QUALITY - A MOLECULAR-DYNAMICS STUDY*. Macromolecules, 1993. **26**(12): p. 3108-3117.
13. Soga, K.G., H. Guo, and M.J. Zuckermann, *Polymer brushes in a poor solvent*. Europhysics Letters, 1995. **29**(7): p. 531-536.
14. Yan, L.T. and X.J. Zhang, *Dissipative particle dynamics simulations on overcharged cylindrical polyelectrolyte brushes with multivalent counterions*. Soft Matter, 2009. **5**(10): p. 2101-2108.
15. Borowko, M. and T. Staszewski, *A density functional study of the structure of tethered chains in a binary mixture*. Condensed Matter Physics, 2012. **15**(2).
16. Zhulina, E., C. Singh, and A.C. Balazs, *Behavior of tethered polyelectrolytes in poor solvents*. Journal of Chemical Physics, 1998. **108**(3): p. 1175-1183.
17. Zhulina, E.B., et al., *Coil globule type transitions in polymers .1. Collapse of layers of grafted polymer-chains*. Macromolecules, 1991. **24**(1): p. 140-149.
18. Williams, D.R.M., *Grafted polymers in bad solvents - octopus surface micelles*. Journal De Physique Ii, 1993. **3**(9): p. 1313-1318.

19. Huh, J., et al., *Constrained dewetting of polymers grafted onto a nonadsorbing surface in poor solvents: From pancake micelles to the holey layer*. Macromolecules, 2005. **38**(7): p. 2974-2980.
20. Pattanayek, S.K., T.T. Pham, and G.G. Pereira, *Nano-pattern formation via grafted polymers in poor solvents*. Current Applied Physics, 2006. **6**(3): p. 571-574.
21. Mercurieva, A.A., et al., *Wetting phase diagrams of a polyacid brush with a triple point*. Physical Review E, 2006. **74**(3).
22. Tagliazucchi, M., M.O. de la Cruz, and I. Szleifer, *Self-organization of grafted polyelectrolyte layers via the coupling of chemical equilibrium and physical interactions*. Proceedings of the National Academy of Sciences of the United States of America, 2010. **107**(12): p. 5300-5305.
23. Carrillo, J.M.Y. and A.V. Dobrynin, *Morphologies of Planar Polyelectrolyte Brushes in a Poor Solvent: Molecular Dynamics Simulations and Scaling Analysis*. Langmuir, 2009. **25**(22): p. 13158-13168.
24. Wang, K., R.A. Zangmeister, and R. Levicky, *Equilibrium Electrostatics of Responsive Polyelectrolyte Monolayers*. Journal of the American Chemical Society, 2009. **131**(1): p. 318-326.
25. Guo, P.J., R. Sknepnek, and M.O. de la Cruz, *Electrostatic-Driven Ridge Formation on Nanoparticles Coated with Charged End-Group Ligands*. Journal of Physical Chemistry C, 2011. **115**(14): p. 6484-6490.
26. Barr, S.A. and A.Z. Panagiotopoulos, *Conformational transitions of weak polyacids grafted to nanoparticles*. Journal of Chemical Physics, 2012. **137**(14): p. 144704.
27. Johner, A. and C.M. Marques, *Can a polymer brush trap a wetting layer*. Physical Review Letters, 1992. **69**(12): p. 1827-1830.
28. Marko, J.F., *Polymer brush in contact with a mixture of solvents*. Macromolecules, 1993. **26**(2): p. 313-319.
29. Birshtein, T.M. and Y.V. Lyatskaya, *Theory of the collapse-stretching transition of a polymer brush in a mixed-solvent*. Macromolecules, 1994. **27**(5): p. 1256-1266.
30. Lyatskaya, Y.V., et al., *Analytical self-consistent-field model of weak polyacid brushes*. Macromolecules, 1995. **28**(10): p. 3562-3569.
31. Lyatskaya, Y. and A.C. Balazs, *Phase separation of mixed solvents within polymer brushes*. Macromolecules, 1997. **30**(24): p. 7588-7595.
32. Birshtein, T.M., E.B. Zhulina, and A.A. Mercurieva, *Amphiphilic polymer brush in a mixture of incompatible liquids*. Macromolecular Theory and Simulations, 2000. **9**(1): p. 47-55.
33. Mercurieva, A.A., et al., *Amphiphilic polymer brush in a mixture of incompatible liquids. Numerical self-consistent-field calculations*. Macromolecules, 2000. **33**(3): p. 1072-1081.
34. Birshtein, T.M., A.A. Mercurieva, and E.B. Zhulina, *Deformation of a polymer brush immersed in a binary solvent*. Macromolecular Theory and Simulations, 2001. **10**(7): p. 719-728.
35. Leermakers, F.A.M., et al., *Effect of a polymer brush on capillary condensation*. Langmuir, 2001. **17**(14): p. 4459-4466.
36. Mercurieva, A.A., et al., *An annealed polyelectrolyte brush in a polar-nonpolar binary solvent: Effect of pH and ionic strength*. Macromolecules, 2002. **35**(12): p. 4739-4752.

37. Hershkovits, E., A. Tannenbaum, and R. Tannenbaum, *Scaling aspects of block co-polymer adsorption on curved surfaces from nonselective solvents*. Journal of Physical Chemistry B, 2008. **112**(17): p. 5317-5326.
38. DeGennes, P., *Scaling theory of polymer adsorption*. J. Phys. France, 1976. **37**(12): p. 1445-1452.
39. Amoskov, V.M., T.M. Birshtein, and A.A. Mercurieva, *SCF theory of a polymer brush immersed into a multi-component solvent*. Macromolecular Theory and Simulations, 2006. **15**(1): p. 46-69.
40. Derouet, D. and C.N.H. Thuc, *Synthesis of polyisoprene-grafted silicas by free radical photopolymerisation of isoprene initiated from silica surface*. Journal of Rubber Research, 2008. **11**(2): p. 78-96.
41. Gauthier, M. and A. Munam, *Cross-linked latex particles grafted with polyisoprene as model rubber-compatible fillers*. Polymer, 2009. **50**(25): p. 6032-6042.
42. Nakano, T., D. Kawaguchi, and Y. Matsushita, *Anisotropic Self-Assembly of Gold Nanoparticle Grafted with Polyisoprene and Polystyrene Having Symmetric Polymer Composition*. Journal of the American Chemical Society, 2013. **135**(18): p. 6798-6801.
43. Cui, L., et al., *In situ synthesis of polyisoprene/grafted single-walled carbon nanotube composites*. Polymer Journal, 2013. **45**(8): p. 834-838.
44. Booth, C., et al., *Studies in the thermodynamics of polymer-liquid systems: Part I—Natural rubber and polar liquids*. Polymer, 1964. **5**: p. 343-370.
45. Eichinger, B.E. and P.J. Flory, *Thermodynamics of polymer solutions. Part 1.—Natural rubber and benzene*. Trans. Faraday Soc., 1968. **64**: p. 2035-2052.
46. Groot, R.D. and P.B. Warren, *Dissipative particle dynamics: Bridging the gap between atomistic and mesoscopic simulation*. Journal of Chemical Physics, 1997. **107**(11): p. 4423-4435.
47. Allen, M.P., Tildesley, D. J, *Computer Simulation of Liquids*. Clarendon, Oxford, 1987.
48. Hoogerbrugge, P.J. and J.M.V.A. Koelman, *Simulating microscopic hydrodynamic phenomena with dissipative particle dynamics*. Europhysics Letters, 1992. **19**: p. 155-160.
49. Vishnyakov, A., D.S. Talaga, and A.V. Neimark, *DPD Simulation of Protein Conformations: From alpha-Helices to beta-Structures*. Journal of Physical Chemistry Letters, 2012. **3**(21): p. 3081-3087.
50. Lee, M.T., A. Vishnyakov, and A.V. Neimark, *Calculations of Critical Micelle Concentration by Dissipative Particle Dynamics Simulations: the Role of Chain Rigidity*. Journal of Physical Chemistry B, 2013. **117**: p. 10304-10310.
51. Jorgensen, W.L., J.D. Madura, and C.J. Swenson, *Optimized Intermolecular Potential Functions for Liquid Hydrocarbons* J. Am. Chem. Soc., 1984. **106**: p. 6638-6646.
52. Lyubartsev, A.P. and A. Laaksonen, *M.DynaMix - a scalable portable parallel MD simulation package for arbitrary molecular mixtures*. Computer Physics Communications, 2000. **128**(3): p. 565-589.
53. Derr, E.L., *Selectivity and Solvency in Aromatics Recovery*. Ind. Eng. Chem. Process Des. Dev., 1964. **3**: p. 394-399.
54. Vishnyakov, A., M.T. Lee, and A.V. Neimark, *Prediction of the Critical Micelle Concentration of Nonionic Surfactants by Dissipative Particle Dynamics Simulations*. Journal of Physical Chemistry Letters, 2013. **4**(5): p. 797-802.
55. Widom, B., *Some Topics in the Theory of Fluids*. J. Chem. Phys., 1963. **39**: p. 2808-2812.

56. Wijmans, C.M., B. Smit, and R.D. Groot, *Phase behavior of monomeric mixtures and polymer solutions with soft interaction potentials*. Journal of Chemical Physics, 2001. **114**(17): p. 7644-7654.
57. Dolan, J.W. and L.R. Snyder, *Gradient Elution Chromatography*, in *Encyclopedia of Analytical Chemistry*, R.A. Meyers, Editor. 2006, Wiley.
58. Brun, Y. and P. Alden, *Gradient separation of polymers at critical point of adsorption*. Journal of Chromatography A, 2002. **966**(1): p. 25-40.
59. Bolz, R.E., *Handbook of Tables for Applied Engineering Science* 1973: CRC Press.
60. Hoover, W.G., *Canonical Dynamics - Equilibrium Phase-Space Distributions*. Physical Review A 1985. **31**(3): p. 1695-1697.
61. Nose, S., *A Molecular-Dynamics Method for Simulations in the Canonical Ensemble*. Molecular Physics, 1984. **52**(2): p. 255-268.
62. Sandia_National_Lab. *LAMMPS Benchmarks*. 2013; Available from: http://lammps.sandia.gov/bench.html.